Original Article

A fast volumetric 4D-MRI with sub-second frame rate for abdominal motion monitoring and characterization in MRI-guided radiotherapy

Jing Yuan, Oi Lei Wong, Yihang Zhou, Kin Yin Chueng, Siu Ki Yu

Medical Physics and Research Department, Hong Kong Sanatorium & Hospital, Hong Kong, China.

Correspondence to: Jing Yuan, PhD. Medical Physics and Research Department, Hong Kong Sanatorium & Hospital, 8/F, Li Shu Fan Block, 2 Village Road, Happy Valley, Hong Kong, China. Email: jyuanbwh@gmail.com.

Background: To propose a fast volumetric 4D-MRI based on 3D pulse sequence acquisition for abdominal motion monitoring and characterization in MRI-guided radiotherapy (MRgRT).

Methods: A 3D spoiled gradient echo sequence volumetric interpolated breath-hold examination (VIBE) [repetition time/echo time (TR/TE) =0.53/1.57 ms, flip-angle =5°, receiver bandwidth (RBW) =1,400 Hz/voxel] based 4D-MRI acquisition, accelerated by 4-fold controlled aliasing in parallel imaging results in higher acceleration (CAIPIRINHA), named CAIPIRINHA-VIBE 4D-MRI, was implemented on a 1.5T MRI simulator (MR-sim) and applied for abdominal imaging of nine healthy volunteers under free breathing. One hundred and forty-four dynamics of the entire abdomen volume (56 slices), in total 8,064 (144×56) images with a voxel size of 2.7×2.7×4.0 mm^3, were acquired in 89 s for 4D-MRI. This CAIPIRINHA-VIBE 4D-MRI was qualitatively compared with a 2D half-Fourier acquisition single-shot turbo spin-echo (2D-HASTE) based 4D-MRI. The motions of liver dome, kidney and spleen were analyzed using the CAIPIRINHA-VIBE 4D-MRI data. The kidney motion was quantitatively characterized in terms of motion range and the correlations between left and right kidneys.

Results: CAIPIRINHA-VIBE 4D-MRI was successfully conducted in all subjects. CAIPIRINHA-VIBE 4D-MRI exhibited much higher effective volumetric temporal resolution (0.615 *vs.* ~5 s/volume) and better reconstructed volume consistency than 2D-HASTE 4D-MRI. CAIPIRINHA-VIBE 4D-MRI was able to characterize the respiratory motion of abdominal organs simultaneously in three orthogonal directions, and could potentially be used for whole abdomen deformable motion tracking. Renal motion range was most pronounced in superior-inferior (SI) direction (L: 10.03±2.65 mm; R: 10.38±2.80 mm), significantly larger (P<0.001) than that in anterior-posterior (AP) and the least in left-right (LR) directions. Right kidney had significantly larger mobility (4.18±2.19 *vs.* 2.32±1.34 mm, P=0.045) than left kidney in AP, but not in LR and SI directions. The Pearson correlation coefficients r between left and right kidney motion were 0.5063 (P=0.164), 0.6624 (P=0.052) and 0.5752 (P=0.105) in LR, AP and SI correspondingly. The correlation of renal motion in SI and AP was found significant in right kidney (r=0.843, P=0.004) but not in left kidney (r=0.467, P=0.205).

Conclusions: A fast volumetric 4D-MRI was implemented for abdominal motion monitoring in MRgRT. A sub-second volumetric temporal resolution of 0.615 s, covering the entire abdomen, was demonstrated for respiratory motion monitoring and characterization. This technique holds potentials for MRgRT applications.

Keywords: Radiotherapy (RT); four-dimensional magnetic resonance imaging (4D-MRI); MRI-guided radiotherapy (MRgRT); respiratory motion; motion monitoring

Submitted May 01, 2019. Accepted for publication Jun 27, 2019.
doi: 10.21037/qims.2019.06.23
View this article at: http://dx.doi.org/10.21037/qims.2019.06.23

© Quantitative Imaging in Medicine and Surgery. All rights reserved.

Introduction

Imaging-guided radiotherapy (IGRT) has dramatically improved the accuracy of the radiation delivery in radiotherapy with the reduced systematic and random errors. Improved RT treatment outcomes by using IGRT have been evidenced by many clinical trials (1,2). However, on the other hand, the current IGRT techniques are still far from optimal when they are applied for tumors in the thorax and abdomen in the presence of respiratory motion, which is often irregular in patients and could be up to several centimeters in the superior-to-inferior (SI) direction (3-6). The moving tumors and organs-at-risk (OARs) with respiration are often poorly visualized on X-ray-based images in IGRT, limited by the intrinsic low soft tissue contrast of X-ray-based imaging. Meanwhile, the imaging dose could be intensive if continuous real-time motion monitoring is conducted using X-ray imaging. MRI-guided-radiotherapy (MRgRT or MRIgRT) has been proposed and is gaining more interests for better tumor motion characterization and management, potentially further improving the radiation delivery accuracy to the target and reducing the toxicity to the OARs, by taking the advantages of non-ionizing radiation nature of MRI as well as its superior and versatile soft-tissue image contrasts (7-15). 4D-MRI (four dimensions are anatomy in 3D space plus respiration in time), which is usually understood as the respiratory-correlated or respiratory-cardiac-correlated dynamic MRI in radiation oncology rather than the time-resolved dynamic MRI in diagnostic radiology, is a potentially powerful tool to characterize the respiratory-induced motion of the tumors and OARs in treatment planning, and to monitor the organ motion in real time and guide radiation delivery during treatment (16-18).

In recent years, numerous 4D-MRI techniques have been proposed in literatures for both treatment planning and image guidance. In terms of image acquisition, current 4D-MRI techniques use 2D pulse sequences, either in interleaved multi-slice or orthogonal cine acquisition mode, much more frequently than 3D pulse sequences, in particular if designed aiming for motion monitoring or image guidance purpose (18-32). 2D pulse sequences acquire images slice by slice, in either sequential or interleaved ordering. The temporal resolution in terms of slice frame rate (measured in second per slice) of 2D acquisition could easily reach the level of <0.5 s/slice. Meanwhile, the in-plane spatial resolution of 2D acquisition is usually better than that of 3D acquisition, although its slice thickness could not be too thin, e.g., <2 mm. Otherwise, slice profile and signal-to-noise ratio (SNR) could be deteriorated. As such, the voxel size of 2D acquisition is usually anisotropic and the through-plane spatial resolution is lower than its in-plane resolution. Furthermore, a variety of 2D pulse sequences are clinically available to obtain different MR image contrasts, also explaining the popularity of 2D acquisition for 4D-MRI. However, on the other hand, 2D acquisition for 4D-MRI is associated with some intrinsic problems due to it slice-by-slice acquisition procedure. For treatment planning, despite of the fast slice frame rate of 2D acquisition, its temporal resolution in terms of volume frame rate (measured in second per volume) is much lower (usually in tens of seconds, depending on slice numbers in the volume, slice temporal resolution as well as slice acquisition ordering) than the respiratory rate (with a normal respiration cycle of 3–5 s). As such, the slices in the imaged volume are acquired at the different respiratory phases in different respiratory cycles. When the slices are sorted for each respiratory phase and reconstructed in 3D views, the anatomies could suffer severely from the problem of structure discontinuity, such as structure missing, stitching edge, and/or overlapping slices, in particular for the situations of poor breath control and irregular respiration pattern in patients, although numerous dedicated algorithms have been proposed for 4D-MRI respiratory-phase sorting and reconstruction (20,21,23,28,29,31). For treatment guidance purpose, volumetric motion monitoring in real-time is technically impractical by using 2D pulse sequences, so cine acquisition of a few number of representative slices (e.g., 1–3 slices) in a single view (usually sagittal or coronal) or orthogonal views (axial-sagittal, axial-coronal, etc.) is usually conducted (7,19). Consequently, only the motion in the sub-volume of interest could be monitored, but it might not faithfully represent the ground truth motion of the entire volume, and thus compromises radiation delivery accuracy.

4D-MRI acquisition using 3D pulse sequences theoretically has some advantages over using 2D pulse sequences. First, it is easier to obtain isotropic voxel size and spatial resolution. Second, 3D pulse sequences acquire the MRI data on the basis of continues volume instead of slice-by-slice, alleviating some technical difficulties of respiratory-phase sorting in 2D acquisition and avoiding volume discontinuity. Third, non-Cartesian acquisition trajectory could be better designed and utilized in 3D pulse sequences, making them less sensitive to respiratory and thus reducing motion artifacts. A number of dedicated 3D

© Quantitative Imaging in Medicine and Surgery. All rights reserved.

Figure 1 The illustration of a volunteer setup with arms-up that is immobilized with the personalized vacuum cushion in this study.

acquisition techniques have been proposed for 4D-MRI and excellent image quality has been achieved for treatment planning purpose (32-38). Lastly, the geometric fidelity of 3D acquisition is better than that of 2D acquisition, in particular in the through-plane direction, which is critically demanded for RT applications (39). However, in practice, 3D acquisition is rarely proposed and used for motion monitoring during the treatment. One most important reason is that 3D acquisition is thought to be too slow (in the order of tens of seconds) to capture the respiratory motion. Also because of the much lower acquisition speed than the respiratory rate, MRI images acquired under free breathing using 3D pulse sequences for real-time motion monitoring, in which scenario no respiratory gating or navigating is allowable, could exhibit pronounced motion artifacts and thus affect tracking accuracy.

Thus, in this study, we prompt to propose and develop a fast 4D-MRI based on 3D pulse sequence acquisition to achieve sub-second volumetric frame rate (VFR), particularly aiming for whole abdominal motion monitoring and characterization in MRgRT applications.

Methods

A total of nine healthy volunteers (aged 34.33±5.77 years), were prospectively recruited for this ethics approved study. Informed consent was obtained from each subject.

Scan setup and MRI acquisition

All MR scans were conducted with a 1.5-Tesla MRI-simulator (MAGNETOM Aera, Siemens Healthineers, Erlangen, Germany) on which the patient table was overlaid with a flat RT-indexed coach-top (Diacor, Salt Lake City, Utah, USA). Subjects were immobilized with arms-up on a personalized vacuum cushion overlaid on the flat couch top using the lock bars. Subjects were aligned with a well-calibrated 3D positioning laser (DORADOnova MR3T, LAP GmbH Laser Applikationen, Luneburg, Germany). An 18-channel body matrix coil was placed anterior to the subject as close as possible but without touching using two-coil bridges (Orfit Industries, Belgium). The embedded spine coil on the patient couch was also enabled for image acquisition. A typical volunteer setup is illustrated in *Figure 1*.

A 3D spoiled gradient-echo pulse sequence, volumetric interpolated breath-hold examination (VIBE) on Siemens MRI, was chosen for acquisition (40,41). Transversal MRI acquisition was adopted to comply with the 4D-CT commonly used in RT, and also to reduce the effect of faster cardiac motion than the respiratory motion on the introduction of motion artifacts in 4D-MRI images. To achieve the aiming sub-second VFR, a couple of approaches were applied for acceleration. Controlled aliasing in parallel imaging results in higher acceleration (CAIPIRINHA) (42,43) with an acceleration factor of 4 was applied. A very short repetition time (TR) of 1.57 ms was achieved by using wide receiver bandwidth (RBW), maximal gradient slew-rate and asymmetric echo. This imaging protocol [transversal, field of view (FOV) =350 (FE, frequency encoding) ×262.5 (PE, phase encoding) ×224 (SE, slice encoding) mm, FE in left-right (LR) direction, slices =56, slice thickness =4 mm, matrix size =128×128×56, echo time (TE)/TR =0.53/1.57 ms, flip-angle =5°, RBW =1,400 Hz/voxel, CAIPIRINHA factor =4, partial Fourier factor =6/8, partial echo factor =6/8] resulted in a temporal resolution of 615 ms per volume (56 slices), i.e., 1.63 fps (frames-per-second) and a reconstructed voxel size of 2.7×2.7×4.0 mm^3. 3D geometric correction was enabled on console for acquisition. This 4D-MRI protocol, named CAIPIRINHA-VIBE 4D-MRI hereafter, was applied for abdominal imaging of 9 healthy volunteers under free breathing. One hundred and forty-four dynamics of the volume, in total 8,064 (144×56) images, were acquired in 89 s. During free-breathing acquisition, respiratory profile was recorded using a pressure transducer bellow with a temporal resolution of 50 ms. The time stamp of each data point in the recorded respiratory profile was also logged.

A 2D pulse sequence, i.e., half-Fourier acquisition single-shot turbo spin-echo (HASTE), based 4D-MRI acquisition, which was used in another 4D-MRI study in our center, was also conducted for the qualitative comparison of image

© Quantitative Imaging in Medicine and Surgery. All rights reserved.

quality with 3D acquisition. This 2D acquisition also covered the abdomen, and was conducted in the coronal view to obtain high volumetric temporal resolution. The imaging parameters were: coronal, FOV =384×384 mm, interleaved slice acquisition, FE in superior-inferior (SI) direction, slices =30, echo train length (ETL) =55, slice thickness =6 mm, slice gap =0, matrix size =192×192, TE/TR =44/165 ms, flip-angle =90°, refocusing-angle =110°, RBW =1,000 Hz/voxel, generalized autocalibrating partially parallel acquisitions (GRAPPA) factor =3, voxel size = 2×2×6 mm), which yielded a slice temporal resolution of 0.165 s/slice and an effective volume temporal resolution of ~5 s/volume (0.165 s ×30 =4.95 s). Due to its 2D interleaved slice acquisition nature, only 2D geometric correction was enabled on console for acquisition.

Data analysis

All acquired MR data were exported as DICOM images and processed off-line using 3D Slicer version 4.5.0 (http://www.slicer.org) (44). The time stamp of each DICOM image in the 4D-MRI data was registered to the closest time stamp of the logged respiratory profile.

The motions of liver dome, kidney and spleen were analyzed using the CAIPIRINHA-VIBE 4D-MRI data. Each anatomy was manually masked on the MRI data of the first time frame (i.e., the first dynamics) as reference. The anatomies in the following time frames were rigidly registered to those of the reference. The transformation matrix was recorded to calculate the displacement of each anatomy relative to the reference with time in three orthogonal directions, i.e., SI, anterior-posterior (AP) and LR directions. We also conducted B-spline based deformable registration in the whole abdomen using the 4D-MRI data to illustrate the feasibility of generation of 3D deformable vector field (DVF) map associated with respiratory motion.

For illustration purpose, kidney motion was quantitatively characterized in terms of its motion range in three orthogonal directions. Motion characteristics of the left (L) and right (R) kidney were compared using *t*-test. Correlations between two kidney motions were analyzed using Pearson correlation. A P value of 0.05 or smaller was considered statistically significant.

Results

The CAIPIRINHA-VIBE 4D-MRI was successfully conducted in all nine healthy volunteers.

The reformatted CAIPIRINHA-VIBE 4D-MRI images of a volunteer were illustrated and compared to the 2D HASTE 4D-MRI in the same volunteer in *Figure 2*. Even at a relatively fast respiratory cycle of 3.4±0.4 s (mean ± Std.) of this volunteer, the respiration induced blurring was observable but minor at the liver dome in SI direction in sagittal and coronal views (*Figure 2*). There was no observable ghosting artifact in the CAIPIRINHA-VIBE 4D-MRI images. Meanwhile, the faster cardiac motion did not induce artifacts in the transversal abdomen images. In contrast, HASTE 4D-MRI images had better spatial resolution in the coronal view due to the smaller in-plane voxel size (2.0×2.0 *vs.* 2.7×2.7 mm^2), but exhibited obvious stitching artifacts on the reformatted sagittal and transversal images due to its much slower effective VFR (~5 *vs.* ~0.6 s/volume) and the interleaved slice acquisition order.

Figure 3 illustrates the translational displacements of liver dome, kidney and spleen relative to the first-time frame (in mm) in three orthogonal directions in a volunteer with a relatively fast respiratory cycle of 3.4±0.4 s, along with the logged respiratory curve (in arbitrary unit). The respiratory motion ranges of liver dome, kidneys and spleen in the three orthogonal directions were illustrated in *Table 1*. The 3D DVF map of the whole abdomen (frame 2 relative to frame 1) in the same subject were shown in *Figure 4*, illustrating the potential technical possibility of voxel-wise whole abdomen motion tracking for the treatment guidance in MRgRT.

Renal motion was characterized and denoted in *Table 2*. Substantial inter-subject and inter-respiratory-cycle variations were observed in kidney motion. For both kidneys, translational motion range was most pronounced in SI (L: 10.03±2.65 mm; R: 10.38±2.80 mm), significantly larger (P<0.001) than that in AP and the least in LR. Right kidney had significantly larger mobility (4.18±2.19 *vs.* 2.32±1.34 mm, P=0.045) than left kidney in AP, but not in LR and SI. The Pearson correlation coefficients r between left and right kidney motion were 0.5063 (P=0.164), 0.6624 (P=0.052) and 0.5752 (P=0.105) in LR, AP and SI correspondingly, all insignificant but strongest in AP. The correlation of renal motion in SI and AP was found significant in right kidney (r=0.843, P=0.004) but not in left kidney (r=0.467, P=0.205).

Discussion

We proposed a CAIPIRINHA-VIBE 4D-MRI with a fast

© Quantitative Imaging in Medicine and Surgery. All rights reserved.

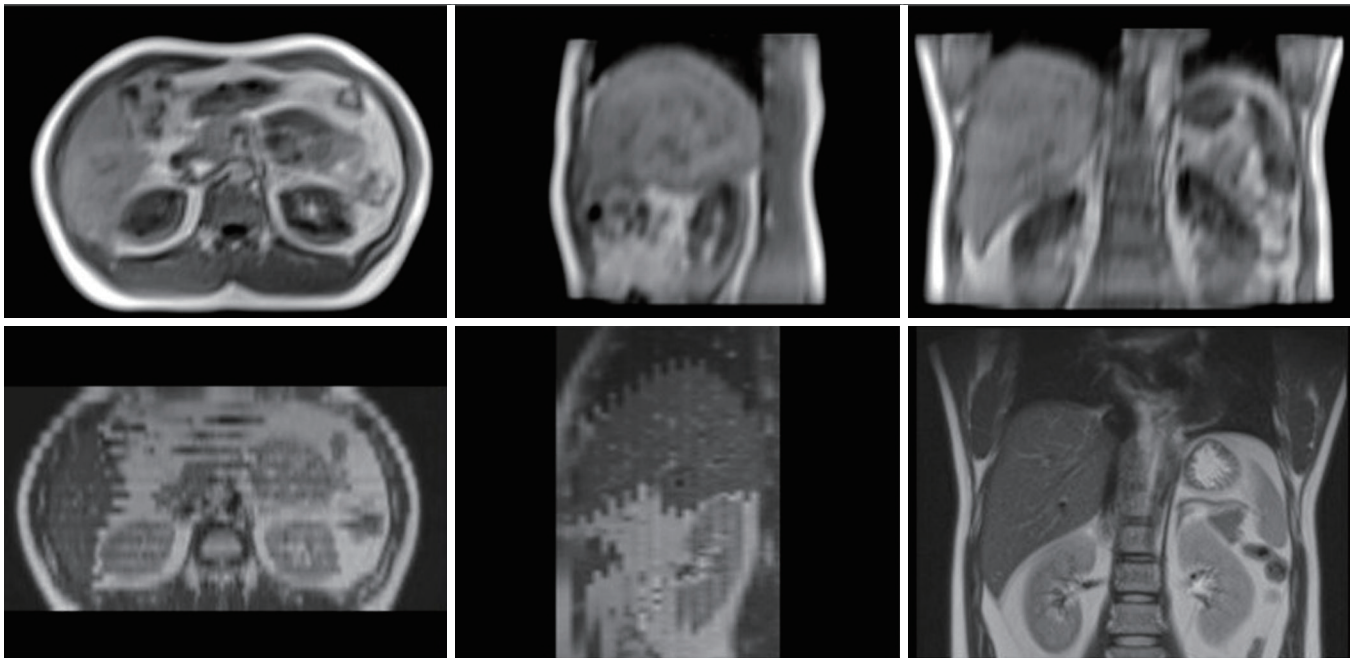

Figure 2 The reformatted CAIPIRINHA-VIBE 4D-MRI images (upper row) of a volunteer in comparison with the 2D-HASTE 4D-MRI images (lower row) in the same volunteer. CAIPIRINHA, controlled aliasing in parallel imaging results in higher acceleration; VIBE, volumetric interpolated breath-hold examination; HASTE, half-Fourier acquisition single-shot turbo spin-echo.

volumetric temporal resolution for MRgRT applications. A VFR of 1.63 fps was illustrated, potentially enabling of whole abdomen motion monitoring and characterization in MRgRT.

This 3D acquisition based CAIPIRINHA-VIBE 4D-MRI has some advantages over the conventionally used 2D acquisition based 4D-MRI in the literature. In addition to the theoretical advantages mentioned in the introduction section, a major advantage of CAIPIRINHA-VIBE 4D-MRI is its much faster VFR than the normal 2D acquisition, such as the 2D-HASTE 4D-MRI as used in this study for comparison. Assuming the normal respiratory cycle of 3–5 s, 5 to 8 frames of the whole abdomen data could be acquired within a single respiratory cycle by the CAIPIRINHA-VIBE 4D-MRI. As comparison, for the 2D-HASTE 4D-MRI, which is considered very fast in terms of its short TR and slice temporal resolution (165 ms) for 2D sequences, only 0.6–1 frame of the abdomen could be obtained within a single respiratory cycle due to its effective volumetric temporal resolution of ~5 s/volume. With the increase of slice numbers, the volumetric temporal resolution of 2D acquisition is inverse-proportionally decreased. As such, the slices in the entire abdomen volume might be acquired at the different respiratory phases in different respiratory cycles. Taking account of inter-respiratory-cycle variability, the reconstructed abdomen volume suffers from volume inconsistency and discontinuity. Furthermore, a 2D pulse sequence has to acquire slices in the interleaved ordering to avoid the slice cross talk artifacts, which inevitably leads to the pronounced stitching artifacts, in particular in the SI direction, the most pronounced respiratory motion direction. The high VFR of CAIPIRINHA-VIBE 4D-MRI could also greatly simplify the post-processing of 4D-MRI data, such as the complicated respiratory amplitude or phase sorting algorithms, and considerably reduce the commonly observed artifacts of missing slices and stitching edge of the reconstructed 4D-MRI data. However, on the other hand, it should be noted that 4D-MRI based on 3D sequence acquisition works on k-space or sequence design instead of sorting images directly, as used in 2D sequence acquisition. Motion artifact usually shows as volume discontinuity with image sorting method based on 2D sequence acquisition. For 3D sequence acquisition, the motion affects more on k-space than on image space, which could be considered as the volume discontinuity artifact in k-space. After Fourier transform of k-space data, the discontinuity artifact in k-space turns to be blurring issue in the image space. In other words, the motion artifact migrates from imaging

© Quantitative Imaging in Medicine and Surgery. All rights reserved.

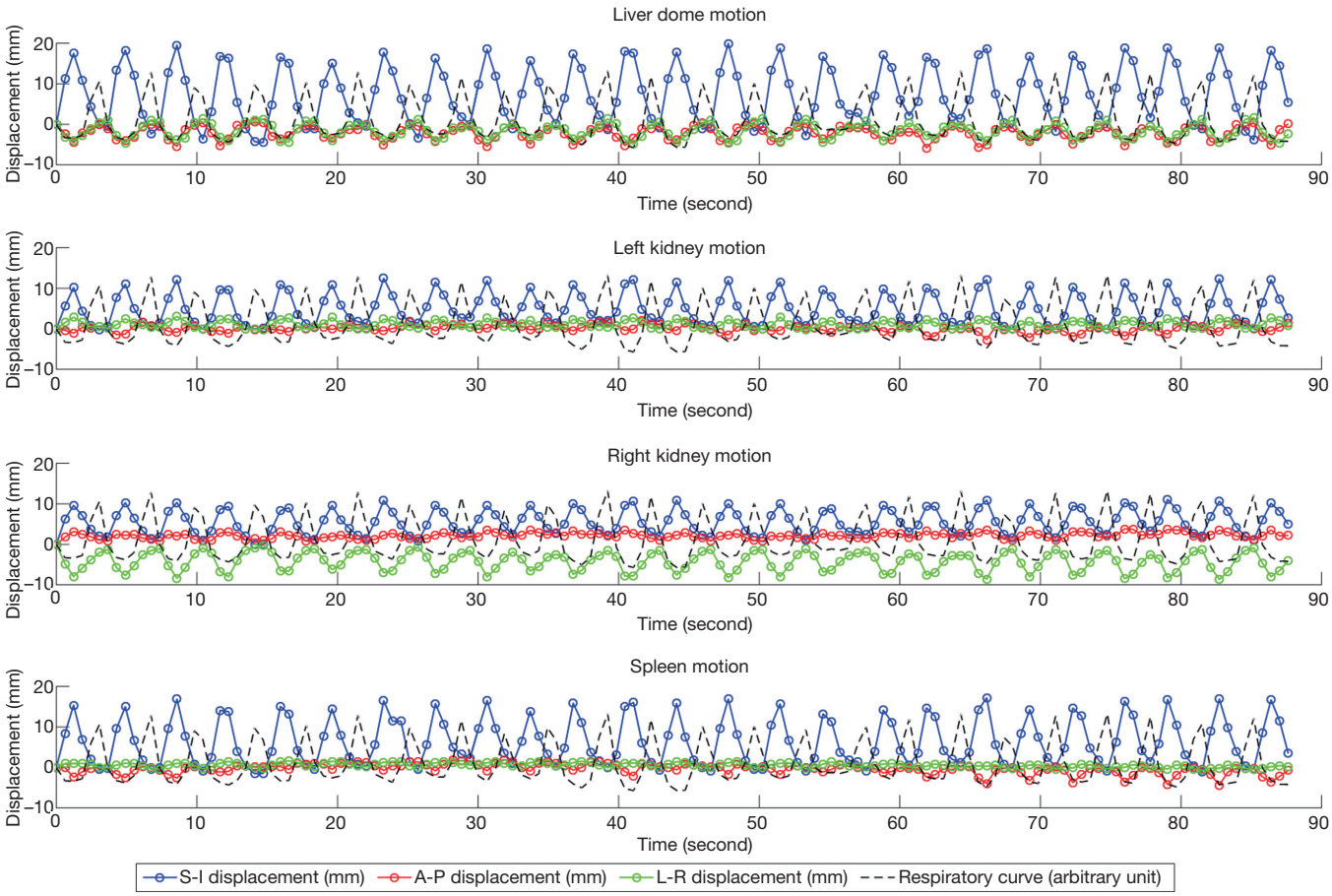

Figure 3 The translation motion of liver dome, kidneys and spleen relative to the first time frame (in mm) in superior-inferior (SI), anterior-posterior (AP) and left-right (LR) directions in a volunteer with a relatively fast averaged respiratory cycle of ~3.4±0.4 s (mean ± Std), along with the logged respiratory curve (in arbitrary unit). Displacements towards S, A and L are defined as positive. The peak of respiratory curve indicates end inhalation and the bottom of respiratory curve indicates end exhalation.

Table 1 The translational motion range of liver dome, kidneys and spleen in the three orthogonal directions (LR, AP, SI) of a single volunteer

Motion range anatomy	LR			AP			SI		
	Min (mm)	Max (mm)	Mean ± Std. (mm)	Min (mm)	Max (mm)	Mean ± Std. (mm)	Min (mm)	Max (mm)	Mean ± Std. (mm)
Liver dome	3.35	6.13	4.86±0.75	2.85	5.77	4.66±0.75	14.95	23.25	19.50±2.06
Left kidney	1.86	3.10	2.38±0.37	0.57	2.73	1.56±0.67	9.18	12.14	10.83±0.88
Right kidney	4.88	7.77	6.52±0.78	0.65	2.47	1.58±0.55	6.60	10.07	8.49±0.93
Spleen	0.20	1.46	0.96±0.39	1.38	4.28	2.64±0.91	14.14	17.93	16.27±1.14

LR, left-right; AP, anterior-posterior; SI, superior-to-inferior.

space to k-space when 3D sequence acquisition is used, showing but in the different pattern.

For the purpose of treatment guidance, CAIPIRINHA-VIBE 4D-MRI could simultaneously monitor the respiratory motion of the entire imaged volume in all three orthogonal directions, greatly alleviating the limitations

© Quantitative Imaging in Medicine and Surgery. All rights reserved.

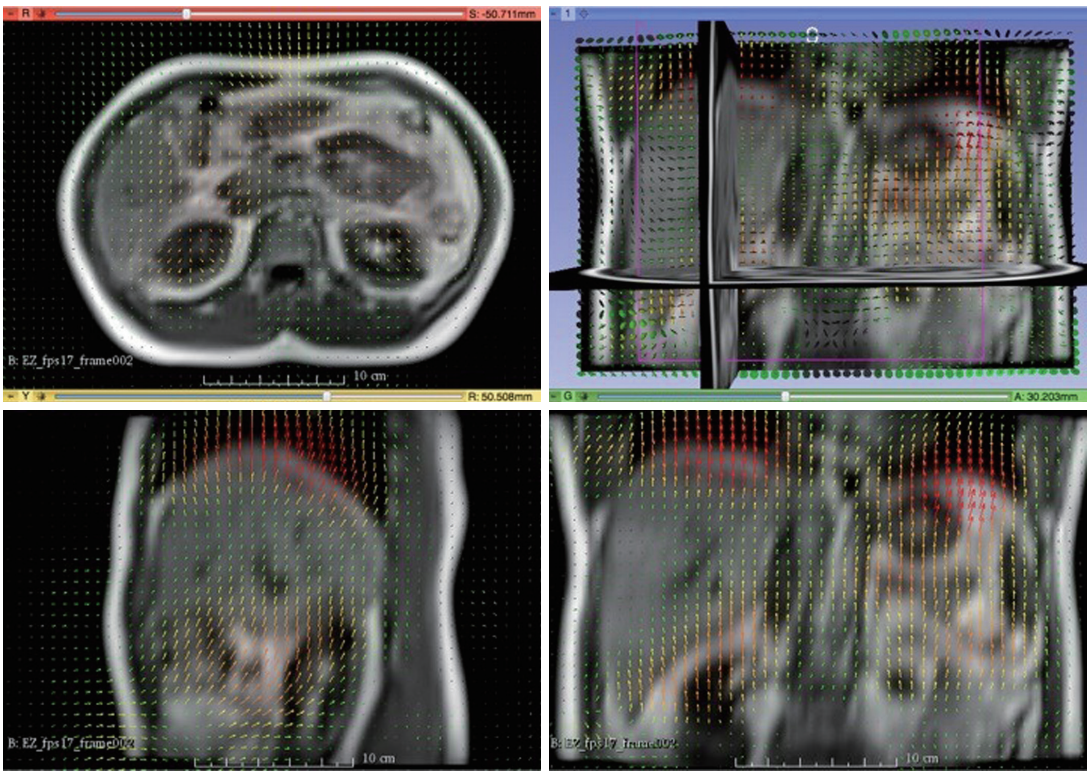

Figure 4 The 3D deformable vector field (DVF) mapping of the whole abdomen (frame 2 relative to frame 1) in the same subject as in *Figure 3*.

of cine MRI acquisition of a few number of slices (e.g., 1–3 slices, the target motion has to be under-sampled in its volume) in a single view (which could only monitor the motion in the two in-plane directions) or orthogonal views (which is associated with saturation band artifact, and motion in the three directions is not retrieved at the same time), without compromising the temporal resolution. Last but not least, VIBE sequence, or their equivalent on other MRI platforms, and CAIPIRINHA acceleration are widely available on many MRI scanners in their clinical libraries, so CAIPIRINHA-VIBE 4D-MRI acquisition protocol could be straightforwardly implemented and readily applied, without using dedicated pulse sequence programming and customized K-space reconstruction algorithms.

The proposed fast 4D-MRI could be further extended. Its volumetric temporal resolution could be further increased straightforwardly by reducing the imaged volume and/or its matrix size, when targeting for small volume tracking. This fast 4D-MRI could also be implemented in other novel fast 3D sequences less sensitive to motion, such as non-Cartesian 3D pulses sequences, and combined with advanced acceleration techniques like compressed sensing to pursue higher spatial-temporal resolution (45,46). It could be also straightforwardly applied in pelvis 4D-MRI for the monitoring and tracking of other motions like intestinal peristalsis.

On the other hand, the proposed 4D-MRI technique also has its limitations. To achieve the fast volumetric temporal resolution, the spatial resolution and image contrast were inevitably somewhat compromised. However, it was reported in literature that the relatively large voxel size (e.g., $5\times5\times5$ mm^3) of 3D imaging, even with low SNR, might not necessarily much compromise the registration accuracy, even in the presence of undersampling artifacts (47-49). The choices of 3D pulse sequences for fast 4D-MRI acquisition are relatively limited. 3D spin-echo sequences might not be appropriate due to its much longer TR and possibly high specific absorption rate (SAR). As such, the use of gradient echo sequences might limit and compromise the image contrasts that could be obtained, most of which are mainly T1-weighted, and make the images more prone to field inhomogeneity and tissue susceptibility. We only illustrated VIBE in this study but other 3D gradient echo sequences, such as balanced steady state free precession (bSSFP),

© Quantitative Imaging in Medicine and Surgery. All rights reserved.

Table 2 The respiratory translation motion of the left and right kidneys (in mm) in SI, AP, LR and 3D directions for each of the 9 volunteers

Subject #	Motion range (Mean ± Std. in mm)							
	Left kidney				Right kidney			
	LR	AP	SI	3D	LR	AP	SI	3D
1	2.50±0.56	0.97±0.48	7.42±1.41	7.91±1.47	1.94±0.44	0.37±0.25	7.03±1.17	7.31±1.22
2	0.54±0.25	2.20±0.31	11.98±0.96	12.20±0.97	3.39±0.60	5.27±1.06	13.15±2.04	14.23±2.71
3	0.22±0.11	0.46±0.80	7.52±0.99	7.58±0.97	1.28±0.19	5.24±0.71	8.79±0.74	10.33±0.83
4	2.38±0.37	1.56±0.67	10.83±0.88	11.22±0.90	6.52±0.78	1.58±0.55	8.49±0.93	10.84±1.11
5	1.40±0.23	2.54±0.48	7.23±1.17	7.81±1.17	1.04±0.28	3.30±0.53	8.63±1.33	9.31±1.41
6	5.39±1.40	3.28±0.68	15.30±2.82	16.61±2.86	4.10±0.54	5.75±0.95	11.55±0.91	13.56±1.18
7	1.23±0.32	1.54±0.53	9.38±1.15	9.61±1.14	0.29±0.18	3.19±0.34	8.05±0.58	8.67±0.57
8	3.09±0.52	4.10±0.95	11.43±1.82	12.30±2.17	3.11±1.60	6.75±1.60	15.21±2.38	17.05±2.56
9	0.28±0.25	4.23±1.08	9.21±2.42	10.17±2.52	1.12±0.36	6.19±1.54	12.54±2.82	14.04±3.19
Cohort	1.89±1.67	2.32±1.34	10.03±2.65	10.60±2.90	2.53±1.95	4.18±2.19	10.38±2.80	11.70±3.18

LR, left-right; AP, anterior-posterior; SI, superior-to-inferior.

might also be feasible to obtain T2/T1-weighted image contrast (50). For treatment planning purpose, the proposed fast 4D-MRI might not be valuable in the original treatment planning for target and OARs delineation due to its limited spatial resolution and compromised image contrast. In this scenario, other strategies of 3D acquisition could be applied. Some researchers have developed 4D-MRI based on 3D sequence acquisition and retrospective K-space self-gating and sorting. High spatial and high temporal resolution was retrospectively obtained for better delineation and respiratory phase sorting (51,52). On the contrary, our proposed method might be useful for fractional 4D-MRI acquisition to characterize the respiratory motion on the treatment day and compare it to that in the original plan for treatment adaptation purpose (13,53,54). For treatment guidance purpose, there are still some critical technical issues that have to be overcome in order to perform motion monitoring, tracking and delivery guidance in real time (55). One most critical issue is the significant latency between the fast image acquisition and the relatively slow on-line image reconstruction. It was observed that a time lag of >20 s occurred from the starting of image acquisition to the first reconstructed image pop-up on MRI console. Other issues include the image data storage and transfer, as well as real-time visualization and processing. With a great amount of data acquired in a short time, i.e., 56 MR images within 615 ms, or 8,064 MR images within 89 s, the data storage on the scanner could quickly full for continuous motion monitoring. In order to achieve real-time motion tracking and radiation delivery guidance, much more powerful computation capability for image visualization, segmentation, registration and interaction with accelerator is critically demanded.

This CAIPIRINHA-VIBE 4D-MRI technique could be potentially used for various scenarios in RT applications. It could be used to investigate and characterize the organ motion simultaneously in three dimensions with respiration, such as motion range, velocity, positional probability distribution (PPD) as well as their inter-respiratory-cycle, inter-subject, and inter-fractional repeatability, potentially helpful to better determine the anisotropic margin of planning target volume (PTV) in three directions as well as the more appropriate motion management strategy. Although the proposed fast 4D-MRI might be of limit value in the task of accurate target and OAR delineation, it should be useful for setting the margins by assessing the 3D motion trajectories of the tumor. Another appropriate scenario to use this fast technique is for daily 4D-MRI acquisition to assess whether the respiratory motion on the treatment day is much deviated from that in the treatment planning, and then determine the treatment adaptation strategy (54). One great potential of this technique should be in the online MRgRT motion monitoring and tracking, provided that technical challenges such as on-line image reconstruction,

© Quantitative Imaging in Medicine and Surgery. All rights reserved.

visualization and data storage etc., are well addressed, particularly for those large and irregular-shaped tumors whose motion could not be fully sampled and faithfully revealed by the 2D cine MR acquisition.

This study has limitations. First, this study only recruited a small number of healthy volunteers instead of real patients. As such, visibility and motion characterization of tumors by using this 4D-MRI protocol could not be assessed. Meanwhile, the image blurring due to the collection of k-space data at different time points might compromise the visualization of structures and the characterization of motion to some degree. As such, the proposed method, in its current form, might not be ideal for structure delineation in the treatment planning, so need to further developed. Theoretically, this fast 4D-MRI could be implemented in the coronal view to obtain higher volumetric temporal resolution, while the effect of cardiac motion on the image quality is yet to be investigated. In all nine healthy volunteers in this study, the CAIPIRINHA-VIBE 4D-MRI obtained stable and reproducible image qualities in the presence of inter-subject and intra-subject respiratory pattern differences. However, the robustness of this 4D-MRI in the presence of faster and/or irregular respiration and other motions, e.g., cough, needs to be further studied in real patient cohorts. Some imaging parameters in this study were restricted on the console in the clinical mode. For example, the maximum allowable time frame number was 144, which restricted the total duration of the motion monitoring in this study by using this technique. The comparison of CAIPIRINHA-VIBE 4D-MRI with 2D-HASTE acquisition in this study was just for qualitative illustration purpose, but not for rigorous quantitative assessment. The residual MRI geometric distortion even after applying 3D geometric distortion correction and its influence on positional accuracy of motion monitoring need to be further carefully investigated. The proposed fast 4D-MRI was implemented on an MR-sim instead of the online MRgRT facilities, such as the integrated MR-LINAC. The related work is under way.

In conclusion, a fast volumetric 4D-MRI based on 3D pulse sequence acquisition was implemented and proposed for abdominal motion monitoring and characterization in MRgRT. A sub-second volumetric temporal resolution of 0.615 s, or an fps of 1.63, covering the entire abdomen, was achieved and demonstrated for respiratory motion characterization. This technique holds potentials for a number of MRgRT applications.

Acknowledgments

None.

Footnote

Conflicts of Interest: The authors have no conflicts of interest to declare.

Ethical Statement: This study was approved by the Institutional Research Ethics Committee (RC-2015-09) of Hong Kong Sanatorium & Hospital. Informed consent was obtained from each subject.

References

1. Verellen D, De Ridder M, Storme G. A (short) history of image-guided radiotherapy. Radiother Oncol 2008;86:4-13.
2. Dawson LA, Jaffray DA. Advances in image-guided radiation therapy. J Clin Oncol 2007;25:938-46.
3. Bissonnette JP, Balter PA, Dong L, Langen KM, Lovelock DM, Miften M, Moseley DJ, Pouliot J, Sonke JJ, Yoo S. Quality assurance for image-guided radiation therapy utilizing CT-based technologies: a report of the AAPM TG-179. Med Phys 2012;39:1946-63.
4. Potters L, Gaspar LE, Kavanagh B, Galvin JM, Hartford AC, Hevezi JM, Kupelian PA, Mohiden N, Samuels MA, Timmerman R, Tripuraneni P, Vlachaki MT, Xing L, Rosenthal SA; American Society for Therapeutic Radiology and Oncology; American College of Radiology. American Society for Therapeutic Radiology and Oncology (ASTRO) and American College of Radiology (ACR) practice guidelines for image-guided radiation therapy (IGRT). Int J Radiat Oncol Biol Phys 2010;76:319-25.
5. Li G, Citrin D, Camphausen K, Mueller B, Burman C, Mychalczak B, Miller RW, Song Y. Advances in 4D medical imaging and 4D radiation therapy. Technol Cancer Res Treat 2008;7:67-81.
6. Langen KM, Jones DT. Organ motion and its management. Int J Radiat Oncol Biol Phys 2001;50:265-78.
7. Mutic S, Dempsey JF. The ViewRay system: magnetic resonance-guided and controlled radiotherapy. Semin Radiat Oncol 2014;24:196-9.
8. Lagendijk JJ, Raaymakers BW, Van den Berg CA, Moerland MA, Philippens ME, van Vulpen M. MR guidance in radiotherapy. Phys Med Biol 2014;59:R349-69.
9. Kupelian P, Sonke JJ. Magnetic resonance-guided adaptive

© Quantitative Imaging in Medicine and Surgery. All rights reserved.

radiotherapy: a solution to the future. Semin Radiat Oncol 2014;24:227-32.
10. Bostel T, Nicolay NH, Grossmann JG, Mohr A, Delorme S, Echner G, Häring P, Debus J, Sterzing F. MR-guidance--a clinical study to evaluate a shuttle- based MR-linac connection to provide MR-guided radiotherapy. Radiat Oncol 2014;9:12.
11. Raaymakers BW, Lagendijk JJ, Overweg J, Kok JG, Raaijmakers AJ, Kerkhof EM, van der Put RW, Meijsing I, Crijns SP, Benedosso F, van Vulpen M, de Graaff CH, Allen J, Brown KJ. Integrating a 1.5 T MRI scanner with a 6 MV accelerator: proof of concept. Phys Med Biol 2009;54:N229-37.
12. Lagendijk JJ, Raaymakers BW, Raaijmakers AJ, Overweg J, Brown KJ, Kerkhof EM, van der Put RW, Hårdemark B, van Vulpen M, van der Heide UA. MRI/linac integration. Radiother Oncol 2008;86:25-9.
13. van Herk M, McWilliam A, Dubec M, Faivre-Finn C, Choudhury A. Magnetic Resonance Imaging-Guided Radiation Therapy: A Short Strengths, Weaknesses, Opportunities, and Threats Analysis. Int J Radiat Oncol Biol Phys 2018;101:1057-60.
14. Pollard JM, Wen Z, Sadagopan R, Wang J, Ibbott GS. The future of image-guided radiotherapy will be MR guided. Br J Radiol 2017;90:20160667.
15. Oelfke U. Magnetic Resonance Imaging-guided Radiation Therapy: Technological Innovation Provides a New Vision of Radiation Oncology Practice. Clin Oncol (R Coll Radiol) 2015;27:495-7.
16. Stemkens B, Paulson ES, Tijssen RHN. Nuts and bolts of 4D-MRI for radiotherapy. Phys Med Biol 2018;63:21TR01.
17. von Siebenthal M, Szekely G, Gamper U, Boesiger P, Lomax A, Cattin P. 4D MR imaging of respiratory organ motion and its variability. Phys Med Biol 2007;52:1547-64.
18. Blackall JM, Ahmad S, Miquel ME, McClelland JR, Landau DB, Hawkes DJ. MRI-based measurements of respiratory motion variability and assessment of imaging strategies for radiotherapy planning. Phys Med Biol 2006;51:4147-69.
19. Seregni M, Paganelli C, Lee D, Greer PB, Baroni G, Keall PJ, Riboldi M. Motion prediction in MRI-guided radiotherapy based on interleaved orthogonal cine-MRI. Phys Med Biol 2016;61:872-87.
20. van de Lindt TN, Fast MF, van der Heide UA, Sonke JJ. Retrospective self-sorted 4D-MRI for the liver. Radiother Oncol 2018;127:474-80.
21. van de Lindt T, Sonke JJ, Nowee M, Jansen E, van Pelt V, van der Heide U, Fast M. A Self-Sorting Coronal 4D-MRI Method for Daily Image Guidance of Liver Lesions on an MR-LINAC. Int J Radiat Oncol Biol Phys 2018;102:875-84.
22. Uh J, Krasin MJ, Li Y, Li X, Tinkle C, Lucas JT Jr, Merchant TE, Hua C. Quantification of Pediatric Abdominal Organ Motion With a 4-Dimensional Magnetic Resonance Imaging Method. Int J Radiat Oncol Biol Phys 2017;99:227-37.
23. Liu Y, Yin FF, Chen NK, Chu ML, Cai J. Four dimensional magnetic resonance imaging with retrospective k-space reordering: a feasibility study. Med Phys 2015;42:534-41.
24. Du D, Caruthers SD, Glide-Hurst C, Low DA, Li HH, Mutic S, Hu Y. High-quality t2-weighted 4-dimensional magnetic resonance imaging for radiation therapy applications. Int J Radiat Oncol Biol Phys 2015;92:430-7.
25. Yamashita H, Yamashita M, Futaguchi M, Takenaka R, Shibata S, Yamamoto K, Nomoto A, Sakumi A, Kida S, Kaneko Y, Takenaka S, Shiraki T, Nakagawa K. Individually wide range of renal motion evaluated by four-dimensional computed tomography. Springerplus 2014;3:131.
26. Sawant A, Keall P, Pauly KB, Alley M, Vasanawala S, Loo BW Jr, Hinkle J, Joshi S. Investigating the feasibility of rapid MRI for image-guided motion management in lung cancer radiotherapy. Biomed Res Int 2014;2014:485067.
27. Heerkens HD, van Vulpen M, van den Berg CA, Tijssen RH, Crijns SP, Molenaar IQ, van Santvoort HC, Reerink O, Meijer GJ. MRI-based tumor motion characterization and gating schemes for radiation therapy of pancreatic cancer. Radiother Oncol 2014;111:252-7.
28. Brix L, Ringgaard S, Sorensen TS, Poulsen PR. Three-dimensional liver motion tracking using real-time two-dimensional MRI. Med Phys 2014;41:042302.
29. Tryggestad E, Flammang A, Han-Oh S, Hales R, Herman J, McNutt T, Roland T, Shea SM, Wong J. Respiration-based sorting of dynamic MRI to derive representative 4D-MRI for radiotherapy planning. Med Phys 2013;40:051909.
30. Eccles CL, Patel R, Simeonov AK, Lockwood G, Haider M, Dawson LA. Comparison of liver tumor motion with and without abdominal compression using cine-magnetic resonance imaging. Int J Radiat Oncol Biol Phys 2011;79:602-8.
31. Cai J, Chang Z, Wang Z, Paul Segars W, Yin FF. Four-dimensional magnetic resonance imaging (4D-MRI) using image-based respiratory surrogate: a feasibility study. Med

© Quantitative Imaging in Medicine and Surgery. All rights reserved.

Phys 2011;38:6384-94.
32. Kirilova A, Lockwood G, Choi P, Bana N, Haider MA, Brock KK, Eccles C, Dawson LA. Three-dimensional motion of liver tumors using cine-magnetic resonance imaging. Int J Radiat Oncol Biol Phys 2008;71:1189-95.
33. Breuer K, Meyer CB, Breuer FA, Richter A, Exner F, Weng AM, Ströhle S, Polat B, Jakob PM, Sauer OA, Flentje M, Weick S. Stable and efficient retrospective 4D-MRI using non-uniformly distributed quasi-random numbers. Phys Med Biol 2018;63:075002.
34. Kumar S, Rai R, Stemmer A, Josan S, Holloway L, Vinod S, Moses D, Liney G. Feasibility of free breathing Lung MRI for Radiotherapy using non-Cartesian k-space acquisition schemes. Br J Radiol 2017;90:20170037.
35. Deng Z, Pang J, Yang W, Yue Y, Sharif B, Tuli R, Li D, Fraass B, Fan Z. Four-dimensional MRI using three-dimensional radial sampling with respiratory self-gating to characterize temporal phase-resolved respiratory motion in the abdomen. Magn Reson Med 2016;75:1574-85.
36. Yang W, Fan Z, Tuli R, Deng Z, Pang J, Wachsman A, Reznik R, Sandler H, Li D, Fraass BA. Four-Dimensional Magnetic Resonance Imaging With 3-Dimensional Radial Sampling and Self-Gating-Based K-Space Sorting: Early Clinical Experience on Pancreatic Cancer Patients. Int J Radiat Oncol Biol Phys 2015;93:1136-43.
37. Feng L, Grimm R, Block KT, Chandarana H, Kim S, Xu J, Axel L, Sodickson DK, Otazo R. Golden-angle radial sparse parallel MRI: combination of compressed sensing, parallel imaging, and golden-angle radial sampling for fast and flexible dynamic volumetric MRI. Magn Reson Med 2014;72:707-17.
38. Buerger C, Prieto C, Schaeffter T. Highly efficient 3D motion-compensated abdomen MRI from undersampled golden-RPE acquisitions. MAGMA 2013;26:419-29.
39. Walker A, Liney G, Metcalfe P, Holloway L. MRI distortion: considerations for MRI based radiotherapy treatment planning. Australas Phys Eng Sci Med 2014;37:103-13.
40. Rofsky NM, Lee VS, Laub G, Pollack MA, Krinsky GA, Thomasson D, Ambrosino MM, Weinreb JC. Abdominal MR imaging with a volumetric interpolated breath-hold examination. Radiology 1999;212:876-84.
41. McKenzie CA, Lim D, Ransil BJ, Morrin M, Pedrosa I, Yeh EN, Sodickson DK, Rofsky NM. Shortening MR image acquisition time for volumetric interpolated breath-hold examination with a recently developed parallel imaging reconstruction technique: clinical feasibility. Radiology 2004;230:589-94.
42. Yu MH, Lee JM, Yoon JH, Kiefer B, Han JK, Choi BI. Clinical application of controlled aliasing in parallel imaging results in a higher acceleration (CAIPIRINHA)-volumetric interpolated breathhold (VIBE) sequence for gadoxetic acid-enhanced liver MR imaging. J Magn Reson Imaging 2013;38:1020-6.
43. Breuer FA, Blaimer M, Heidemann RM, Mueller MF, Griswold MA, Jakob PM. Controlled aliasing in parallel imaging results in higher acceleration (CAIPIRINHA) for multi-slice imaging. Magn Reson Med 2005;53:684-91.
44. Fedorov A, Beichel R, Kalpathy-Cramer J, Finet J, Fillion-Robin JC, Pujol S, Bauer C, Jennings D, Fennessy F, Sonka M, Buatti J, Aylward S, Miller JV, Pieper S, Kikinis R. 3D Slicer as an image computing platform for the Quantitative Imaging Network. Magn Reson Imaging 2012;30:1323-1341.
45. Lustig M, Donoho D, Pauly JM. Sparse MRI: The application of compressed sensing for rapid MR imaging. Magn Reson Med 2007;58:1182-95.
46. Baron CA, Dwork N, Pauly JM, Nishimura DG. Rapid compressed sensing reconstruction of 3D non-Cartesian MRI. Magn Reson Med 2018;79:2685-92.
47. Stemkens B, Tijssen RH, de Senneville BD, Heerkens HD, van Vulpen M, Lagendijk JJ, van den Berg CA. Optimizing 4-dimensional magnetic resonance imaging data sampling for respiratory motion analysis of pancreatic tumors. Int J Radiat Oncol Biol Phys 2015;91:571-8.
48. Roujol S, Ries M, Moonen C, de Senneville BD. Automatic nonrigid calibration of image registration for real time MR-guided HIFU ablations of mobile organs. IEEE Trans Med Imaging 2011;30:1737-45.
49. Glitzner M, de Senneville BD, Lagendijk JJ, Raaymakers BW, Crijns SP. On-line 3D motion estimation using low resolution MRI. Phys Med Biol 2015;60:N301-10.
50. Santini F, Wetzel SG, Bock J, Markl M, Scheffler K. Time-resolved three-dimensional (3D) phase-contrast (PC) balanced steady-state free precession (bSSFP). Magn Reson Med 2009;62:966-74.
51. Han F, Zhou Z, Cao M, Yang Y, Sheng K, Hu P. Respiratory motion-resolved, self-gated 4D-MRI using rotating cartesian k-space (ROCK). Med Phys 2017;44:1359-68.
52. Han F, Zhou Z, Du D, Gao Y, Rashid S, Cao M, Shaverdian N, Hegde JV, Steinberg M, Lee P, Raldow A, Low DA, Sheng K, Yang Y, Hu P. Respiratory motion-resolved, self-gated 4D-MRI using Rotating Cartesian K-space (ROCK): Initial clinical experience on an MRI-guided radiotherapy system. Radiother Oncol

© Quantitative Imaging in Medicine and Surgery. All rights reserved.

2018;127:467-73.
53. Yoganathan SA, Maria Das KJ, Agarwal A, Kumar S. Magnitude, Impact, and Management of Respiration-induced Target Motion in Radiotherapy Treatment: A Comprehensive Review. J Med Phys 2017;42:101-15.
54. Hunt A, Hansen VN, Oelfke U, Nill S, Hafeez S. Adaptive Radiotherapy Enabled by MRI Guidance. Clin Oncol (R Coll Radiol) 2018;30:711-9.
55. Paganelli C, Whelan B, Peroni M, Summers P, Fast M, van de Lindt T, McClelland J, Eiben B, Keall P, Lomax T, Riboldi M, Baroni G. MRI-guidance for motion management in external beam radiotherapy: current status and future challenges. Phys Med Biol 2018;63:22TR03.

Cite this article as: Yuan J, Wong OL, Zhou Y, Chueng KY, Yu SK. A fast volumetric 4D-MRI with sub-second frame rate for abdominal motion monitoring and characterization in MRI-guided radiotherapy. Quant Imaging Med Surg 2019;9(7):1303-1314. doi: 10.21037/qims.2019.06.23

© Quantitative Imaging in Medicine and Surgery. All rights reserved.